Biogeosciences Discuss., 9, 17651–17706, 2012
www.biogeosciences-discuss.net/9/17651/2012/
doi:10.5194/bgd-9-17651-2012

Biogeosciences Discussions

Field intercomparison of four methane gas analysers suitable for eddy covariance flux measurements

O. Peltola[1], I. Mammarella[1], S. Haapanala[1], G. Burba[2], and T. Vesala[1]

[1]Department of Physics, University of Helsinki, P.O. Box 48, Helsinki 00014, Finland
[2]LI-COR Biosciences, 4421 Superior Street, Lincoln, NE 68504, USA

Received: 22 August 2012 – Accepted: 14 September 2012 – Published: 12 December 2012

Correspondence to: O. Peltola (olli.peltola@helsinki.fi)

Published by Copernicus Publications on behalf of the European Geosciences Union.

Abstract

Performances of four methane gas analyzers suitable for eddy covariance measurements are assessed. The assessment and comparison was performed by analyzing eddy covariance data obtained during summer 2010 (1 April to 26 October) at a pristine fen, Siikaneva, Southern Finland. High methane fluxes with pronounced seasonality have been measured at this fen. The four participating methane gas analyzers are commercially available closed-path units TGA-100A (Campbell Scientific Inc., USA), RMT-200 (Los Gatos Research, USA), G1301-f (Picarro Inc., USA) and an early prototype open-path unit Prototype-7700 (LI-COR Biosciences, USA).

The RMT-200 functioned most reliably throughout the measurement campaign, during low and high flux periods. Methane fluxes from RMT-200 and G1301-f had the smallest random errors and the fluxes agree remarkably well throughout the measurement campaign. Cospectra and power spectra calculated from RMT-200 and G1301-f data agree well with corresponding temperature spectra during a high flux period. None of the gas analysers showed statistically significant diurnal variation for methane flux. Prototype-7700 functioned only for a short period of time, over one month, in the beginning of the measurement campaign during low flux period, and thus, its overall accuracy and long-term performance were not assessed. Prototype-7700 is a practical choice for measurement sites in remote locations due to its low power demand, however if only the performance in this intercomparison is considered, RMT-200 performed the best and is the recommended choice if a new fast response methane gas analyser is needed.

1 Introduction

Prior to 1990's, eddy covariance (EC) measurements of methane flux were impossible due to lack of "fast" gas analyzers needed in order to capture turbulent flux transport at all relevant frequencies, or eddy sizes. However, after the development

BGD
9, 17651–17706, 2012

of fast instruments based on the laser absorption spectroscopy (LAS), studies reporting ecosystem scale EC methane flux measurements started to occur more frequently (e.g. Verma et al., 1992; Suyker et al., 1996; Rinne et al., 2007). The early studies employed instruments which needed continuous maintenance, and whose high-speed resolution was not very high. Furthermore, estimating long term methane balance was quite expensive and laborious task due to substantial need of continuous upkeep. The lasers needed to be cooled to cryogenic temperature in order to function properly, and such cooling was usually done with liquid nitrogen which further increased the maintenance requirements.

Recent advancements in the development of LAS gas analyzers have made sensitive and robust instruments commercially available, and accordingly, the number of gas analyzers applicable for EC measurements increased. The new instruments function at room temperature which drastically decreases maintenance needs. The growing use of LAS gas analyzers for eddy covariance methane flux measurements calls for comparison between the instruments. Tuzson et al. (2010) assessed and intercompared performance of two rather new gas analyzers at a grassland site with an artificially created methane flux. Their gas release experiment lasted the total of eleven days. While they were able to assess if flux magnitude was measured correctly, they were not able to determine instruments' long-term performance in field conditions, which is a key issue for continuous greenhouse gas monitoring.

The objective of this study is to compare and assess the performance of four methane gas analyzers and corresponding methane fluxes. This is done by analyzing methane flux data measured during April–October 2010 at Siikaneva fen, Southern Finland. Four methane gas analyzers and one sonic anemometer were used to acquire four methane flux estimates. Long-term performance is assessed by comparing data coverage and estimates for methane budgets, while short-term performance is assessed by analyzing random and systematic errors in the methane flux, and also, by examining spectral characteristics of turbulent mixing. One of the participating analyzers, TGA-100A (Campbell Scientific Inc., USA) (e.g. Billesbach et al., 1998), is an older

BGD
9, 17651–17706, 2012

closed-path model, and is based on the same principle as the gas analyzers used in the early studies in the 1990's. The two other closed-path models, RMT-200 (Los Gatos Research, USA) (e.g. Bär et al., 2002; Hendriks et al., 2008; Eugster and Pluess, 2010; Tuzson et al., 2010), G1301-f (Picarro Inc., USA), and an early open-path prototype, Prototype-7700 (LI-COR Biosciences, USA) (e.g. McDermitt et al., 2010; Dengel et al., 2011; Detto et al., 2011), are new state-of-the-art instruments. The three closed-path units operated with occasional breaks throughout the measurement campaign, whereas Prototype-7700 malfunctioned permanently at 11 July due to water leakage which damaged internal electronics of the instrument.

2 Materials and methods

2.1 Site description

The gas analyzer intercomparison was carried out between 1 April and 26 October 2010, in Siikaneva fen, Southern Finland (61°49.961′ N, 24°11.567′ E, 160 m a.s.l). Siikaneva is a nutrient-poor oligotrophic open fen. Distance from the study site to the tree line is in north and south directions about 200 m, and several hundred meters in east and west directions (Fig. 1). Surrounding forest consists mainly of Scots pines. Peat depth varies from 2 to 4 m, increasing toward the centre of the site. The surface topography is relatively flat with no pronounced slope (Aurela et al., 2007). Due to the topography and relatively large homogeneous fetch, this location is well-suited for eddy covariance flux measurements. The vegetation at the site consists mainly of sedges (*Eriophorum vaginatum*, *Carex rostrata*, *C. limosa*) and *Sphagnum*-species, namely *S. balticum*, *S. majus* and *S. papillosum*. More about vegetation and carbon gas exchange in the study site can be found in Riutta et al. (2007).

Air temperature during the measurement campaign was on average 11.5 °C, a 2.2 °C warmer than 30-yr average, recorded at a nearby meteorological station (Drebs et al., 2002). July was the hottest month with mean air temperature of 20.7 °C. Peat was not

BGD
9, 17651–17706, 2012

frozen during the whole time period. Accumulated precipitation during the measurement period was 372 mm, while Drebs et al. (2002) reported a value of 429 mm for 30-yr average.

2.2 Measurement system

Micrometeorological measurements systems observing trace gas fluxes usually consist of sonic anemometer and at least one gas analyzer. In Siikaneva site, three-axis sonic anemometer (USA-1, METEK, Germany) was used to measure three wind components and air temperature. CO_2 and H_2O concentrations were measured with a closed-path gas analyzer (LI-7000, LI-COR Biosciences, Lincoln, NE, USA). Sonic anemometer was situated at 2.75 m height above soil surface, and the sampling inlet for LI-7000 was situated 25 cm below the sonic anemometer. The sampling tube consisted of two parts: 16 m long tube with 10 mm inner diameter followed by a 0.8 m long tube with 4 mm inner diameter. The longer part was used to sample air also to some of the methane gas analyzers. Both of the tubes were made of Teflon. The whole sampling line was heated in order to avoid condensation of water vapour on the tube walls. Flow rate in the main intake tube was approximately 24 LPM. Horizontal spatial separation between the sampling tube inlet and sonic probe was approximately 5 cm. Four methane gas analyzers were also installed at the same site, and their characteristics are shown in Table 1 and explained in more detail below. All measurements related to eddy covariance were recorded at the rate of 10 Hz. Supporting meteorological and soil parameters were measured in the vicinity of eddy covariance measurement system.

2.2.1 LI-COR Prototype-7700

Prototype-7700 is an early pre-production prototype of the open-path methane gas analyzer (LI-COR Biosciences, USA). Open-path design does not utilize an intake tube or pump to pull the sampled air into the closed measurement cell; rather the measurements are done in-situ, in an open cell, through which air flows freely moved by

BGD
9, 17651–17706, 2012

the wind. The analyzer employs a 0.47 m long open Herriott cell, with 30 m of optical path length. The analyzer was placed under the sonic anemometer resulting in approximately 10 cm horizontal and 45 cm vertical sensor separation distances. The measurement height was 2.3 m above soil surface and 1.1 m above surface of a wooded structure. Tunable diode laser is utilized to create laser beams in the near-infrared region. Methane concentration is measured by using wavelength modulation spectroscopy (WMS) in order to increase measurement accuracy and reduce the effects of mirror contamination. The concentration is determined by scanning over absorption line near 1.65 µm. This scanning is executed at 1 kHz frequency (McDermitt et al., 2010).

2.2.2 Picarro G1301-f

G1301-f (Picarro Inc., USA) is based on wavelength-scanned cavity ring down spectroscopy (WS-CRDS), which is a modified version of a more traditional CRDS approach (O'Keefe and Deacon, 1988). Picarro G1301-f is a closed-path gas analyzer, with sampled air pulled into the cell via the 16 m long intake tube (same one as for LI-7000). The 0.8 m long tube was attached between the main sampling line and the gas analyzer, and thus, the total length of the sampling line was 16.8 m. The tube inlet with a filter was situated 25 cm below the sonic anemometer, at the measurement height 2.5 m above the soil surface. The analyzer was measuring water vapour and methane concentrations. Due to clogging of an internal filter, it was replaced 26 August with an external Pall Acro 50 filter (PTFE membrane 1 µm, Pall Acro 50).

2.2.3 Los Gatos RMT-200

RMT-200 is also a closed-path methane gas analyzer (Los Gatos Research, USA). It is based on the off-axis integrated cavity output spectroscopy (OA-ICOS), which differs from regular ICOS by the fact that the laser is placed at an angle to the axis of the cavity. A 15 m long Teflon sampling tube 8 mm in diameter was utilized to sample air to

BGD
9, 17651–17706, 2012

the gas analyzer. Vertical and horizontal separation between sonic probe and inlet of the tube was 25 cm and 5 cm, respectively. The measurement height was 2.5 m above soil surface. The tube was not heated but it was situated inside a protective cover next to the heated tube used to sample air for LI-7000 and G1301-f. AcroPak filter (PTFE membrane 0.2 µm, Pall AcroPak 300) was attached to the inlet line, just before the analyser.

2.2.4 Campbell TGA-100A

Campbell TGA-100A closed-path gas analyzer (Campbell Scientific Inc., USA) is based on TDLAS measurement technique applied with tunable lead-salt diode laser. This instrument has been widely used in eddy covariance methane flux measurement studies (e.g. Rinne et al., 2007), and is used in this study as a reference for the three new instruments. The laser was cooled using liquid nitrogen. Air was sampled with 13 m long Teflon tube with 4 mm inner diameter. Air was sucked through a filter (polypropylene/polyethylene membrane 10 µm, Pall 60344). Flow rate in the tube was 14 LPM and the inlet was situated at 2.45 m height above soil surface resulting in 30 cm vertical sensor separation between sonic probe and the inlet. Tube was not heated but the air was dried with a diffusion drier (Nafion PD-1000, Perma pure Inc., USA) located after the inlet. Dew point temperature remained at about −15 to −30 °C. Due to this, WPL terms or spectroscopic corrections were not needed.

2.3 Eddy covariance method

Eddy covariance method was used in measuring the vertical turbulent fluxes of trace gases, sensible and latent heat (Aubinet et al., 2000):

$$H = \overline{\rho_a} c_p \overline{w'T'} \quad (1)$$

$$\mathrm{LE} = \lambda \overline{\rho_a} \overline{w'\chi_v'} \quad (2)$$

$$F_c = \overline{\rho_a} \overline{w'\chi_c'} \quad (3)$$

BGD
9, 17651–17706, 2012

where H and LE are sensible heat and latent heat fluxes, respectively, and F_c is turbulent flux of arbitrary scalar c. λ is defined as latent heat of vaporization of water, χ_v water vapour mass mixing ratio ($kg_{water}/kg_{dry\,air}$), T temperature, $\overline{\rho_a}$ is mean air mass density, c_p is the specific heat at constant pressure and χ_c is mass mixing ratio of scalar c ($kg_{gas}/kg_{dry\,air}$). Here u and v are the two horizontal wind components and w is vertical wind component. Equation (3) can describe flux of any scalar, for instance methane, carbon dioxide, ozone, etc. The fluxes are defined to be positive when directed upwards.

Data was processed with post-processing software EddyUH (http://www.atm.helsinki.fi/~mammarel/Eddy_Covariance/). Measurements were sampled at 10 Hz frequency, and 30-min averaging time was used in calculating the covariances. For the most part, data processing followed the methodology described by Aubinet et al. (2000). First the high frequency eddy covariance data were despiked by comparing two adjacent measurements. If there were over 0.5 ppm difference between two adjacent methane concentration measurements the following point was replaced with the same value as in the previous point. Second, the coordinate rotation was applied: wind components u, v and w were rotated so that u was directed toward mean horizontal wind speed and second rotation set mean vertical wind speed, $\overline{w}$ to zero (Kaimal and Finnigan, 1994). Third, the mean values were removed from the time series using block-averaging method. Fourth, time lag between the concentration and wind measurements induced by the sampling lines was corrected by maximizing the covariance. Fifth, spectral corrections were applied (Sect. 2.3.1). Then, humidity effect on temperature flux $\overline{w'T'}$ was accounted for after Schotanus et al. (1983). As a final step, Webb-Pearman-Leuning (WPL) terms and spectroscopic corrections were applied according to the method presented in Sect. 2.3.2.

Turbulent cospectra and power spectra were obtained by applying Fast Fourier Transform (FFT) to linearly detrended, Hamming-windowed, raw high-frequency eddy covariance data. Cospectra were used to determine frequency response of the measurement systems. Both cospectra and power spectra are analyzed in Sect. 3.2.

BGD
9, 17651–17706, 2012

2.3.1 Spectral corrections

Low and high frequency variations in the measured signal are attenuated due to data acquisition and processing, and by a non-ideal measurement system (e.g. Moore, 1986; Moncrieff et al., 1997; Rannik and Vesala, 1999; Massman, 2000). Detrending of data acts as a high pass filter, thus damping low frequency fluctuations (Rannik and Vesala, 1999). Insufficient length of averaging period may cause additional attenuation of low frequency signal (Finnigan et al., 2003). On the other hand, turbulent transport occurring at high frequencies is attenuated due to measurement system's limited capacity to measure small and rapid turbulent motions. Gas analyzer's time constant, spatial separation between the instruments and line, or volume, averaging effects caused by instrument design affect the attenuation of high frequency fluctuations in the signal. For closed-path gas analyzers the sampling tube and a filter attached to the tube may also have major impact on the measurement system's ability to detect rapid fluctuations in the signal.

Attenuation of low frequency variation was corrected with transfer function (TF_{LF}) after Rannik and Vesala (1999), while attenuation of high frequency variations was corrected with transfer function after Horst (1997):

$$TF_{HF} = \frac{1}{1 + (2\pi f \tau)^2} \quad (4)$$

where f is natural frequency and τ is measurement system-specific coefficient, called response time. τ was determined for each gas analyser experimentally by assuming scalar similarity and comparing normalized temperature and methane cospectra. Magnitude of signal attenuation can be estimated with correction factor CF (Aubinet et al.,

BGD
9, 17651–17706, 2012

2000):

$$\mathrm{CF} = \frac{\int_0^\infty S_{wT}^{\mathrm{model}}(f)\,\mathrm{d}f}{\int_0^\infty \mathrm{TF}_{\mathrm{HF}}(f)\,\mathrm{TF}_{\mathrm{LF}}(f)\,S_{wT}^{\mathrm{model}}(f)\,\mathrm{d}f} \quad (5)$$

where S_{wT}^{model} is the scalar model cospectrum. Now by multiplying measured flux with correction factor CF, the fluxes can be corrected for signal attenuation.

2.3.2 Effect of water vapour and temperature fluctuations on gas concentration measurements

Pressure, temperature and water vapour affect the shape and width of the absorption lines used to deduce gas concentration, and thus, gas concentration measured with a laser may not be equal the real gas concentration. If there is fluctuation, for instance, in the sample gas temperature, it would induce fluctuation in the measured gas concentration even though the real concentration would stay constant. The same reasoning in principle also applies to pressure fluctuations, yet the barometric pressure in eddy flux measurements is usually treated as a constant (Webb et al., 1980). Therefore, only fluctuations in sample temperature and water vapour partial pressure, and the resulting spectroscopic effects, are taken into account.

Spectroscopic effects may cause apparent trace gas fluxes due to the fact that water vapour and temperature fluctuations correlate with fluctuations in trace gas concentrations, and with vertical wind speed at the same time. Since trace gas fluxes are calculated as covariance between gas concentration and vertical wind speed (Sect. 2.3), these spectroscopic effects may induce apparent fluxes. These effects are absorption line-specific features and they also depend on the spectroscopic approach used to

BGD
9, 17651–17706, 2012

measure the gas. Thus, gas analyzers using different absorption lines to deduce the gas concentrations will have difference spectroscopic effects on the measured trace gas flux. This has to be accounted for when the magnitude of apparent fluxes is estimated and corrected.

Spectroscopic effects on measured trace gas fluxes were first described by Lübken et al. in 1991, and later in Burba et al. (2009), Neftel et al. (2010) and Tuzson et al. (2010), and McDermitt et al. (2010) estimated the magnitude of this effect. The latter is based on patent by Burba et al. (2009), and both describe the same correction method. Neftel et al. (2010) and Tuzson et al. (2010) used experimental approach, while Lübken et al. (1991) and McDermitt et al. (2010) determined this effect theoretically. Burba et al. (2009), McDermitt et al. (2010) and LI-7700 manual (LI-COR Inc., 2010) proposed to correct this effect by adjusting the WPL terms (Webb et al., 1980) with appropriate multipliers. This method is presented next. First, they define a dimensionless correction factor $\kappa(T,P)$, which describe how absorption line shape is affected by temperature and pressure. It is derived from parameters given in HITRAN database (Rothman et al., 2009) and basic spectroscopic theory. However, in order to account for changes in absorption line shape caused by water vapour, pressure P needs to be augmented with equivalent pressure P_e (Burch et al., 1962). The trace gas flux, F_c, is calculated then using their Eq. (3) and taking into account the effect of $\kappa(T,P_e)$ in the measured concentration. After some algebra (see LI-7700 manual for details), equation similar to what was suggested by Webb et al. (1980) is achieved:

$$F_c^{\mathrm{corr}} = A\left\{\overline{w'\rho_{\mathrm{cm}}'} + B\mu\frac{\overline{\rho_{\mathrm{cm}}}}{\overline{\rho_a}\lambda}\mathrm{LE} + C\frac{(1+\mu\sigma)\overline{\rho_{\mathrm{cm}}}}{\overline{\rho_a}c_p\overline{T}}H\right\} \quad (6)$$

BGD
9, 17651–17706, 2012

where

$$A = \overline{\kappa} \tag{7}$$

$$B = 1 + \left(1 - 1.46\overline{x_v}\right)\alpha_v \overline{P_e} \frac{\kappa_{P_e}}{\overline{\kappa}} \tag{8}$$

$$C = 1 + \left(1 - \overline{x_v}\right)\overline{T} \frac{\kappa_T}{\overline{\kappa}} + \overline{x_v}(B - 1) \tag{9}$$

and ρ_{cm}, and ρ_a are uncorrected methane and air mass density, respectively, κ_{P_e} and κ_T are the partial derivatives of κ with respect to pressure and temperature, computed at $T = \overline{T}$ and $P_e = \overline{P_e}$, respectively. μ is molar mass of air divided with molar mass of water, σ is mean water vapour density divided with mean air density and x_v is mole fraction of water vapour (mol_{water}/mol_{air}). With this equation spectroscopic effects can be corrected simultaneously with density fluctuation induced errors, i.e. WPL terms.

In a closed-path gas analyzer temperature fluctuations in the sample gas are damped while the gas is transported in the long tube (Leuning and Moncrieff, 1990; Rannik et al., 1997). Thus, air sample temperature is effectively constant in the sampling cell, meaning that the spectroscopic effects and density fluctuation caused by temperature fluctuations may be neglected, and therefore, third term in the right hand side in Eq. (6) may be set to zero. For open-path gas analyzers this cannot be done, and the correction should be applied in its full form.

Neftel et al. (2010) and Tuzson et al. (2010) used slightly different approach in correcting errors induced by spectroscopic effects. This is probably because they used closed-path gas analyzers, and needed to investigate only the effect of water vapour, while Burba et al. (2009) and McDermitt et al. (2010) used open-path gas analyzer and they had to account also for temperature fluctuations. For closed-path gas analyzers spectroscopic effects can be corrected by adding water vapour flux multiplied with certain factor b_{ct} to the measured trace gas flux, i.e.

$$F_c^{SP} = F_c^{meas} + b_{ct} \frac{M_c}{M_v \lambda} LE \tag{10}$$

BGD
9, 17651–17706, 2012

where F_c^{meas} is measured flux (Eq. 3), F_c^{SP} is flux corrected for the spectroscopic effects and M_c and M_v are molar masses of scalar c and water, respectively.

The fundamental difference between these two correction methods is that the former method (Burba et al., 2009; McDermitt et al., 2010) is based on the spectroscopic theory, verified by experiments, while the latter (Neftel et al., 2010) relies on empirical laboratory measurements. In any case, these two correction methods (Eqs. 6 and 10) address the same problem, regardless of the way they are derived, and results are expected to be equivalent to each other.

It should also be reiterated that spectroscopic correction is specific to absorption line, measurements technique and thus measurement device, so value for b_{ct} must be determined for each gas analyser separately. In this study, spectroscopic and WPL terms was performed for Prototype-7700 with Eq. (6). For RMT-200, WPL terms were estimated from Eq. (6) by setting third term on right hand side to zero and $A = B = 1$, while spectroscopic correction was calculated with Eq. (10), with b_{ct} generally adopted after Tuzson et al. (2010) with some modification. Their b_{ct} incorporates both corrections (spectroscopic and WPL) in the same b_{ct} value, and they also state that the spectroscopic correction is approximately 16 % of WPL H_2O-term, so in our study b_{ct} was set to 3.965×10^{-7} $mol_{CH_4}\, mol_{H_2O}^{-1}$, which is 16 % of the value that Tuzson et al. (2010) reported. This value also agrees with our lab results. For RMT-200, instead of maximizing the water vapour flux, values for LE used in spectroscopic correction and WPL terms were calculated using RMT-200 methane time lag, as suggested by Ibrom et al. (2007). For G1301-f the corrections were performed using the method and coefficients presented in Chen et al. (2010). They use second order polynomial function which describes the effect of H_2O on methane concentration. The correction is done point-by-point to the raw data. After 26th of August the instrument was not any more measuring H_2O and thus correction described in Chen et al. (2010) could not anymore be used. After this date only WPL correction could be done to the data. Closed-path gas analyzer TGA-100A was connected to dryer and therefore it was free from cross-sensitivity between measured gas and water vapour and this correction was not needed.

BGD
9, 17651–17706, 2012

2.4 Random error estimation methods

Errors in measurements can be systematic or random. Errors resulting in random uncertainties do not introduce any bias to the calculated flux; rather they decrease reliability of the measurement. Eddy covariance trace gas flux measurements have various sources for random uncertainties. They are related to atmospheric conditions, measurement and data analysis methods and measurement site characteristics (Businger, 1986; Kroon et al., 2010).

According to Kroon et al. (2010) the uncertainty of measured covariance $\overline{w'\chi_c'}$ is dominated by the uncertainty that is related to one-point sampling of the flux. This is due to the fact that they assume that uncertainty due to measurement precision of vertical wind w and concentration c are negligible. One-point uncertainty is linearly proportional to standard deviation of the measured covariance (Businger, 1986) and thus by comparing the standard deviations of covariances, it is possible to compare uncertainties in the four methane flux estimates. The standard deviations of the covariances were calculated according to method proposed by Finkelstein and Sims (2001):

$$\sigma_F = \sqrt{\frac{1}{n_s}\left[\sum_{p=-m}^{m}\hat{\gamma}_{c,c}(p)\,\hat{\gamma}_{w,w}(p) + \sum_{p=-m}^{m}\hat{\gamma}_{w,c}(p)\,\hat{\gamma}_{c,w}(p)\right]} \tag{11}$$

where n_s is the total number of samples in a data set, m is a number samples that is sufficiently large in order to cover the integral timescale (e.g. Stull, 1988) and $\hat{\gamma}_{c,c}$ and $\hat{\gamma}_{c,w}$ are autocovariance and cross-covariance functions, respectively. In this study n_s equals 18 000 due to 10 Hz sampling frequency and 30 min averaging time, m is equal to 200, as suggested by Finkelstein and Sims (2001), and auto- and crosscovariance

BGD
9, 17651–17706, 2012

functions were calculated as

$$\hat{\gamma}_{x,x}(p) = \hat{\gamma}_{x,x}(-p) = \frac{1}{n_s} \sum_{t=1}^{n_s-p} \left(x_t - \overline{x}\right)\left(x_{t+p} - \overline{x}\right) \quad (12)$$

$$\hat{\gamma}_{x,y}(p) = \hat{\gamma}_{y,x}(-p) = \frac{1}{n_s} \sum_{t=1}^{n_s-p} \left(x_t - \overline{x}\right)\left(y_{t+p} - \overline{y}\right) \quad (13)$$

This mathematically rigorous method provides estimates for the random uncertainty in flux measurements for every averaging period. Finkelstein and Sims (2001) argue that this method provides better estimate for the standard deviation of the covariance than previously reported methods. This is due to the fact that it does not assume any kind of cospectral or spectral shapes for the turbulent transport, more like the method is based on direct statistical calculation of variance of covariance.

Absolute value for fractional flux error describing the standard deviations as a fraction of the covariance $\overline{w'\chi_c'}$ were calculated as

$$\mathrm{AFFE} = \left|\frac{\sigma_F}{\overline{w'\chi_c'}}\right| \quad (14)$$

AFFE illustrates how big fraction of the measured flux can be a product of random uncertainty, which is related to sampling and instrumental noise. If AFFE values are below one, the measured flux values are statistically significant.

Random uncertainty related to instrumental noise (σ_{inst}) were estimated with a method proposed by Billesbach (2011). It is based on minimizing the correlation between the time series w and c by randomly shuffling one of them. This corresponds to removing the signal related to turbulent flux from the measurements. After shuffling, covariance between w and c is only related to instrumental noise (Billesbach, 2011).

$$\sigma_{\mathrm{inst}} = \frac{1}{n_s} \sum_{i=1}^{n} w'(i)\chi_{c\,\mathrm{shuf}}'(i) \quad (15)$$

BGD
9, 17651–17706, 2012

where vector $\chi_c{}'_{\text{shuf}}$ contains all the measurements in time series $\chi_c{}'$ but the values are in random order. In this study σ_{inst} was calculated eight times for every 30-min averaging period and the mean of the absolute values of these eight estimates for σ_{inst} were used to estimate random uncertainty related to instrumental noise. σ_{inst} was calculated eight times in order to reduce uncertainty of instrumental noise estimate.

2.5 Gap filling procedure

Several studies have presented different parameterizations for methane flux (e.g. Kroon et al., 2010; Wille et al., 2008; Rinne et al., 2007; Suyker et al., 1996). It seems that the environmental factors controlling methane emissions strongly depend on the measurement site or ecosystem. For instance, Wille et al. (2008) reported strong dependence between mean wind speed and methane flux in their study carried out in an artic tundra ecosystem at Lena river delta; however no clear connection between these two variables were found in our data for the fen. Suyker et al. (1996) reported a dependence of methane flux on water table depth, with 12 day lag, for a boreal fen ecosystem in Canada, which was not found by Rinne et al. (2007) in their fen study.

Exponential dependence between methane flux and peat temperature is commonly used to describe connection between soil microbiological reactions and temperature (Conrad, 1989). In this study methane flux was parameterized using peat temperature measured at 35 cm depth:

$$y = ab^{(x-10)/10} \tag{16}$$

where y is average daily methane flux obtained from the four instruments in $\text{mg}\,\text{m}^{-2}\,\text{h}^{-1}$ and x is peat temperature (°C) at 35 cm depth. Values 1.88 ± 0.03 and 5.34 ± 0.22 were obtained for the coefficients a and b, respectively. The values are given with 95 % confidence limits.

Even though correlation between the measured mean daily methane flux and the used gap filling method is significant ($r^2 = 0.992$) and root mean square error is low

BGD
9, 17651–17706, 2012

(RMSE = 0.17 mg m^{-2} h^{-1}), the parameterisation is not able to capture the high flux periods, which are observed roughly between days 190 and 210 (Fig. 2). Reason for the sudden drop in mean daily methane flux around day 205 is unclear. Rinne et al. (2007) reported similar phenomenon in their study, which was carried out at the same site, and they hypothesized that it might be caused by the fact that the growth of the methanogenic microbe population exceeds the growth in the available substrates, thus limiting the methane production. However, further studies are needed to confirm this hypothesis.

3 Results

3.1 Data coverage

The intercomparison campaign was carried out between 1 April and 26 October 2010. None of the methane gas analyzers operated continuously through the entire period (Fig. 2). The open-path Prototype-7700 was in operation for 33 days in the beginning of the campaign. The prototype was not operational after 5 June 2010, due to improperly sealed enclosure, leading first to a hardware malfunction (reset in sampling rate from 10 Hz to 1 Hz) on 5 June and a few days later, to a permanent water damage on 11 June. The water sealing issue was fixed later in the production model by the manufacturer. However, as a result of the water damage, the only period when the methane flux was measured with the prototype was during relatively small fluxes of about 0.5 mg m^{-2} h^{-1}. Thus, it is difficult to estimate how it would have performed in measuring during medium and high flux periods in the middle of summer, when the flux was around 3–10 mg m^{-2} h^{-1}.

The G1301-f was out of use approximately 40 days in the end of July, beginning of August, when fluxes were largest reaching over 10 mg m^{-2} h^{-1}. Starting from 15 August the pressure regulation of G1301-f measurement cell did not function properly. Reason for this was the obstruction of an internal filter. Due to the fact that the internal

BGD
9, 17651–17706, 2012

filters were difficult to replace with new ones, the clogged internal filter was removed and replaced with an external Pall Acro 50 filter which is easier to handle. From the 26 August onwards the instrument was back in operation. However, reason for the missing data before 15 August is still unclear. One possible cause is that temperature in the cabinet which housed the closed-path gas analyzers was too high by the end of July and beginning of August, which might have caused G1301-f to be unstable, and loose the data. In a better ventilated container this problem may not have occurred. TGA-100A was taken away from the site at the middle of August. The fact that the instruments were not operating continuously at the same time should be kept in mind when examining and assessing the results, especially for the short operating time of Prototype-7700.

Flux data coverage of the four gas analyzers was estimated during a period when they all functioned properly, between 17 April and 17 May. All methane flux data was discarded if friction velocity was below $0.1\,m\,s^{-1}$, resulting in 164 half-hourly points to be discarded between 17 April and 17 May. Magnitude of methane flux showed rapid decrease after friction velocity dropped below this threshold (not shown) as also reported for CO_2 by Goulden et al. (1996) and others.

The post-processing software also examined Prototype-7700 measurements when RSSI (Received Signal Strength Indicator) describing cleanliness of the mirrors had a mean value below threshold of 20. This threshold was reached on 120 half-hours which were then discarded. Also, the amount of spikes, i.e. outliers, in raw CH_4 concentration data and mean half-hourly value of CH_4 concentration were used in detecting and discarding additional erroneous data. These criteria discarded 104 and 6 additional half-hours, respectively. Including discarded sonic anemometer data, the total of 395 half-hours were removed from Prototype-7700 dataset during the selected period, which was approximately 140 half-hourly points more than for the three closed-path gas analyzers (Table 2). On the whole, the open-path prototype produced least amount of data during the selected period mostly due to the fact that the measurements were done in an open cell which is vulnerable to the precipitation.

BGD
9, 17651–17706, 2012

Eddy covariance data were also flagged with three different quality flags according to stationarity criteria proposed by Foken and Wichura (1996). Flags 0, 1 and 2 represent data with good, mediocre and bad quality, respectively. RMT-200 and G1301-f produced the most of high quality flux data (flag 0 in Table 2) during this 30-day-period. Both of them produced data approximately 77 % of time which can be categorized as good data. For TGA-100A this percentage is 61 % and for Prototype-7700 it is 56 %. For RMT-200 and G1301-f the amount of data flagged with 0 has a noticeable diurnal variation: around midday almost all the measurements are flagged with 0, at night the amount of good data is smaller and the amount of data flagged with 1 and 2 slightly increases. The minimum for the amount of data flagged with 0 is reached around 02:30 a.m. when only 45 % of RMT-200 and G1301-f data are flagged with 0. Due to intermittent turbulent mixing at night it is expected for data quality to have a diurnal variation. However, TGA-100A and Prototype-7700 do not show such a pronounced diurnal variation, and the quality is only slightly better at daytime than at night. This might be caused by the fact that the natural diurnal variation of intermittency of turbulent mixing is overshadowed by some other effects that cause the measured methane flux data to be of lower quality independently of the time of day. Low quality is related to the fact that the measured methane flux is non-stationary during an averaging period. This non-stationarity may be caused by instrument related problems, such as contamination of measurement cell (Prototype-7700) or drift in the signal (TGA-100A). Thus it can be argued that the quality of RMT-200 and G1301-f data is dominated by the characteristics of turbulent mixing, while for TGA-100A and Prototype-7700 there are some instrument specific phenomena causing a decrease in the data quality.

3.2 Spectral characteristics

Figure 3 shows ensemble averaged, normalized and frequency weighted cospectra and power spectra received from the four methane gas analyzers. For Prototype-7700 data was selected from period 17 April–17 May while for others data was selected from period 9–29 June. Data was selected according to following criteria: stratification

BGD
9, 17651–17706, 2012

was unstable, data was flagged with quality flag 0, wind speed was between 1.5 $m s^{-1}$ and 4 $m s^{-1}$ and methane flux was directed upwards. In other words, only periods with well-developed turbulence and unstable conditions were selected. It must be pointed out that this selection of data was done for each methane gas analyzer individually and thus the ensemble averaged methane cospectra are not calculated from the same runs, rather the figure shows the ensemble average calculated from best available data for each gas analyzer.

According to scalar similarity assumption, all normalized scalar cospectra, plotted against the normalized frequency n, should collapse into one curve. In other words, temperature and methane cospectra should look the same in Fig. 3. Therefore, by comparing methane cospectra and temperature cospectra with each other, it is possible to assess how well the methane gas analyzers are able to measure methane flux related to different sizes of eddies. Since sonic anemometers can measure the kinematic heat flux and thus scalar cospectra more accurately than the gas analyzers, the temperature cospectra should be closer to the theoretical scalar cospectrum, and can be used as a reference for other scalar cospectra. Overall, all ensemble averaged methane cospectra and temperature cospectra agree well. CH_4 flux cospectra from all four methane gas analyzers follow the temperature cospectra at lower frequencies, but at higher frequency they start to fall below the $w'T'$ cospectra. This damping of high frequency signal is specific to an instrument and setup, and its effect on the magnitude of methane flux can be corrected. This correction and its magnitude are explained in detail in Sect. 3.4.1. From Fig. 3, it is evident that dampening of high frequency signal is most pronounced for RMT-200 cospectra.

Ensemble-averaged and frequency-weighted power spectra of methane and temperature are shown on the right hand side of Fig. 3. All the ensemble averaged methane power spectra are greatly affected by white noise during period 17 April–17 May (shown only for Prototype-7700 in Fig. 3). During this period the methane flux was relatively low, approximately 0.5 $mg m^{-2} h^{-1}$. When the flux is low, variation in measured methane concentration may be greatly affected by noise in the signal, and in open-path devices,

BGD
9, 17651–17706, 2012

by the fluctuations in ambient temperature, humidity and pressure, since the methane signal is small. Thus high frequency fluctuation in methane concentration may be dominated by white noise in closed-path devices, and by white noise, temperature humidity and pressure fluctuations in open-path devices, rather than by a real methane signal. The fact that the signal is dominated by white noise means that the fluctuations at these frequencies in methane concentration time series are resulting from instrumental noise and other sources of random noise and therefore they are not corresponding to real fluctuations in the signal. Thus the smaller the frequency range where white noise dominates the better. The white noise seen in power spectra does not contribute to the covariance due to the fact that white noise in methane concentration measurements does not correlate with vertical wind speed time series; rather it just increases the random error of the measurement.

During period 9–29 June, when Prototype-7700 was already out of operation, the methane fluxes were from 10 to 12 time higher than during the period 17 April–17 May, and the ensemble averaged power spectra seem to follow the temperature power spectra better (the upper three plots on the right hand side in Fig. 3). G1301-f power spectra does not show any sign of white noise, while RMT-200 power spectra starts to be dominated by white noise when $n \approx 2.2$, corresponding to frequency 1.6 Hz. At slightly lower frequencies also dampening of RMT-200 signal can be detected. TGA-100A ensemble averaged methane power spectra starts to deviate from the temperature ensemble averaged power spectra already when the normalized frequency is around 0.4 (0.3 Hz) (Fig. 3). White noise had most significant effect on TGA-100A of all instruments. TGA-100A ensemble averaged power spectra deviated from temperature power spectra also at low frequencies during both periods, possibly as a result of the drift in the signal.

3.3 Random error estimation

The median standard deviations of the covariances related to four methane gas analyzers during two different periods are shown on the left of Fig. 4. The standard deviations represent the uncertainty caused by instrumental noise and one-point sampling

BGD
9, 17651–17706, 2012

of the flux and they were calculated from raw eddy covariance data. TGA-100A and Prototype-7700 give largest standard deviations for the covariances, implying larger random errors. During the first period (17 April–17 May) they gave almost twice the standard deviation of that for RMT-200 and G1301-f. Random error of the flux measurements is related to the magnitude of measured flux, i.e. high flux leads to high random error. Since open-path instruments are subject to the full water vapour and temperature effects, and to the full WPL equation, and closed-path instruments are not subject to these, the raw uncorrected Prototype-7700 methane flux shows uptake of methane in the middle of day, while the closed-path instruments show weak emission. Therefore, random error related to magnitude of the raw flux is expected to be higher for the open-path Prototype-7700 than for the closed-path instruments shown in Fig. 4 (left plot). During the second period (9 June–29 June) the standard deviations were overall approximately five times larger than during the first period. This was expected due to the fact that the measured flux was significantly larger during the second period.

In addition to standard deviations, which describe the random uncertainty caused by sampling and instrumental noise, the random uncertainty caused purely by instrumental noise was estimated according to Eq. (15) (Billesbach, 2011). Magnitude of instrumental noise is a good measure of instrument performance. The mean values are plotted in Fig. 4. Uncertainty caused by instrumental noise increases when the flux magnitude increases. This can be seen if the noise levels during the two periods are compared, because the methane flux was on average larger during the second period. Again, RMT-200 and G1301-f performed the best during both periods by having smallest mean values for the instrumental noise, while TGA-100A had the highest.

Absolute values for fractional flux errors (AFFE) were calculated according to Eq. (11). They describe how the random error behaves relative to methane flux magnitude, regardless of the direction. RMT-200 and G1301-f give the smallest average values for AFFE during the both periods (Fig. 4, central plot). AFFE from Prototype-7700 is approximately 0.03 higher than from RMT-200 or G1301-f. AFFE of TGA-100A

BGD
9, 17651–17706, 2012

was consistently higher than for the other three instruments due to higher standard deviation.

Distribution of AFFE values during the first period (17 April–17 May) is shown in Fig. 5. All the distribution curves show an asymmetric shape: the curves peak at low AFFE values and then they have a tail reaching up to higher AFFE values. From cumulative frequency of occurrence shown on the right in Fig. 5, it is evident that approximately 90 % of the RMT-200 and G1301-f AFFE values are below 0.19 and the most common value is approximately 0.12. The distributions of AFFE values are very narrow; absolute values of fractional flux error values above 0.3 are rarely witnessed.

Distributions of TGA-100A and Prototype-7700 AFFE values are wider than for the two previous gas analyzers. This is evident from the cumulative frequency of occurrence shown in Fig. 5. About 90 % of the AFFE values are below 0.5 for TGA-100A and below 0.63 for Prototype-7700. The most common value for Prototype-7700 is 0.13, while for TGA-100A it is 0.18. The distribution of Prototype-7700 AFFE values peaks at the same place as distribution of RMT-200 and G1301-f values, however high AFFE values are more common for Prototype-7700. Small amount of high AFFE values imply that the instrument is measuring methane concentration precisely most of the time and thus it can be said that the smaller amount of high AFFE values the better. Therefore, according to Fig. 5, RMT-200 and G1301-f perform the best and Prototype-7700 and TGA-100A fall clearly behind the first two in precision.

AFFE of Prototype-7700 and TGA-100A methane flux measurements depend on the magnitude of the flux. Most of the AFFE values are below 0.5, however when the flux falls below $0.2\,\mathrm{mg\,m^{-2}\,h^{-1}}$, the AFFE values start to rise. For RMT-200 and G1301-f such a dependence is not detected. This might be partly caused by the fact that they did not measure as small fluxes as the other instruments and thus the high AFFE values that are related to small fluxes are not detected. If only moments when absolute value of raw uncorrected methane flux was larger than $0.3\,\mathrm{mg\,m^{-2}\,h^{-1}}$ are used, the median AFFE values are 0.12, 0.13, 0.17 and 0.15 for RMT-200, G1301-f, TGA-100A and Prototype-7700, respectively.

BGD
9, 17651–17706, 2012

3.4 Systematic error estimation

Unbiased correct information on the reference magnitude of the real flux is needed in order to estimate how much the measured methane flux deviates from the real methane flux. Such information cannot be obtained, as all the measurements may have errors. Nonetheless, certain measurement system and data processing induced systematic errors have been identified and they can be corrected. These corrections are presented in the following subsections.

3.4.1 Spectral corrections

As mentioned in Sect. 3.2, the high frequency end of methane flux cospectra is usually attenuated, meaning that it falls below temperature flux cospectra. High frequency part of methane flux cospectra divided with temperature cospectra are shown in Fig. 6. Grey line shows transfer function given in Eq. (4) with corresponding response time. This grey line should follow the ensemble averaged methane cospectrum divided with temperature cospectrum (black dots) and the high frequency part of spectral correction can be estimated by integrating over the transfer function.

Response times were estimated experimentally using method presented in Aubinet et al. (2000). As a result, mean response times of 0.16 s, 0.08 s, 0.10 s and 0.16 s were obtained for RMT-200, TGA-100A, G1301-f and Prototype-7700, respectively. These values correspond to cut-off frequencies of 0.64 Hz, 1.28 Hz, 1.02 Hz and 0.64 Hz, respectively. Cut-off frequency corresponds to that frequency where the transfer function equals $2^{-1/2}$, meaning that the flux has been attenuated to approximately 0.7 of the real value at this frequency. TGA-100A has the shortest response time, meaning that it responds the best to changes in methane concentration. However, it must be kept in mind that not only the instrument response, but also the rest of the measurement system (sampling tube and filter, response of sonic anemometer, spatial sensor separation) has an effect on the total system response time. Therefore, the obtained

BGD
9, 17651–17706, 2012

response times describe not only the instrument response, but also the ability of the whole system to measure high frequency turbulent fluctuations.

Long response time of Prototype-7700 is rather surprising. Usually open-path instruments (i.e. LI-7500) have shorter response times than closed-path instruments due to the fact that the high frequency dampening due to the sampling line and filters is not present. Long Prototype-7700 response time might be a result from the fact that it was positioned under the sonic anemometer, substantially below the rest of the intakes, and 1.1 m above the surface of the wood log structure. The 0.45 m vertical separation between the instrument and the sonic anemometer in conjunction with 1.1 m height above the structure likely caused the observed attenuation of high frequency signal. In such situation, the large open sampling cell may not be able to resolve the smallest turbulent eddies. However, in other studies (Detto et al., 2011; McDermitt et al., 2010) the commercial model LI-7700 resolved eddies well.

Magnitudes of the spectral corrections are given in Table 3 as fractions of the raw, uncorrected methane flux. Diurnal variations of data with and without spectral corrections are shown in Fig. 7 for RMT-200 and Prototype-7700. Spectral corrections always increase the absolute value of the flux, regardless of what is the direction of the flux. Spectral corrections are done before adding WPL terms or doing spectroscopic corrections, thus spectrally-corrected fluxes are still affected by density fluctuations and spectroscopic effects. This means that for Prototype-7700, RMT-200 and G1301-f spectral corrections are done for datasets that follow dotted lines in Fig. 7. For Prototype-7700 the corrections increase the magnitude of negative and positive methane fluxes (Table 3 and Fig. 7) during daytime and night time, respectively. Thus spectral corrections partly balance the effect of WPL terms and spectroscopic corrections on Prototype-7700 methane fluxes due to the fact that they have an opposing effect on the flux. If Tables 3 and 4 are compared, it is evident that for Prototype-7700 WPL terms and spectroscopic correction are more important than spectral corrections. The correction has the smallest effect on TGA-100A and G1301-f methane fluxes (Table 3). This is

BGD
9, 17651–17706, 2012

expected due to the fact that they had shorter response time than Prototype-7700 and RMT-200.

3.4.2 Sensitivity to water vapour and temperature fluctuations

TGA-100A was connected to a drier and thus for this instrument no density or spectroscopic corrections are needed. Significance of WPL terms (Webb et al., 1980) and the new spectroscopic correction are assessed for G1301-f, RMT-200 and Prototype-7700 in this section using data obtained between 17 April–17 May.

For open-path gas analyzers the WPL terms are significantly more important than for closed-path instruments, due to the fact that for closed-path gas analyzers the temperature fluctuations are dampened by the sampling tube prior to air sample arrival to the measurement cell. Thus we can expect that the WPL terms and the spectroscopic correction will be larger for Prototype-7700 methane fluxes than for RMT-200 or G1301-f. Spectroscopic and WPL terms were applied according the method presented in Sect. 2.3.2. For Prototype-7700 the coefficients A, B and C in Eq. (6) were obtained from look-up tables distributed with the instrument. These coefficients describe the effect of temperature and water vapour fluctuations on the measured methane concentration. For RMT-200 the coefficient b_{ct} was adopted with modification from Tuzson et al. (2010) and for G1301-f the corrections were done based on the method by Chen et al. (2010). During the measurement campaign the approximate ranges for A, B and C were 0.94 to 0.99, 1.42 to 1.46 and 1.21 to 1.34, respectively. McDermitt et al. (2010) reported that these coefficients should be in the range 0.77–1.00, 1.39–1.42 and 1.28–1.4, respectively. In our study, coefficients B and C are slightly outside the range that McDermitt et al. (2010) reported and therefore the correction might be slightly miscalculated. Reason for the discrepancy between McDermitt et al. (2010) and this study was not found.

WPL terms have a significant influence on the open-path Prototype-7700 methane fluxes. The terms increase the flux by 0.20 $\mathrm{mg\,m^{-2}\,h^{-1}}$, on average. However, this difference has a clear diurnal variation. At daytime (sun's elevation angle larger than 0°),

BGD
9, 17651–17706, 2012

it is approximately 0.37 $mg\,m^{-2}\,h^{-1}$ and at night time (sun's elevation angle below −3°) it is around −0.14 $mg\,m^{-2}\,h^{-1}$, meaning that the correction diminishes the fluxes at night. Spectroscopic correction is not as significant as WPL terms for Prototype-7700 methane fluxes: on average fluxes corrected for the spectroscopic effects and density fluctuations are 0.06 $mg\,m^{-2}\,h^{-1}$ larger than only WPL-corrected fluxes. However, also spectroscopic correction has a diurnal variation and the difference is 0.11 $mg\,m^{-2}\,h^{-1}$ at daytime, while at night time it is −0.04 $mg\,m^{-2}\,h^{-1}$. For the closed-path gas analysers RMT-200 and G1301-f the significance of WPL terms and spectroscopic correction are much smaller as expected for a closed-path design. WPL terms increase the fluxes on average by 0.05 $mg\,m^{-2}\,h^{-1}$ and 0.07 $mg\,m^{-2}\,h^{-1}$, respectively. If daytime and night time are examined separately, this increase is 0.08 $mg\,m^{-2}\,h^{-1}$ and 0.01 $mg\,m^{-2}\,h^{-1}$ for RMT-200 and 0.11 $mg\,m^{-2}\,h^{-1}$ and 0.02 $mg\,m^{-2}\,h^{-1}$ for G1301-f, respectively. Significance of spectroscopic correction is smaller than the significance of WPL terms: on average spectroscopic correction increased the fluxes for RMT-200 and G1301-f by 0.01 $mg\,m^{-2}\,h^{-1}$ and 0.003 $mg\,m^{-2}\,h^{-1}$, respectively. At daytime and night time this increase is 0.02 $mg\,m^{-2}\,h^{-1}$ and 0.003 $mg\,m^{-2}\,h^{-1}$ for RMT-200 and 0.003 $mg\,m^{-2}\,h^{-1}$ and 0.002 $mg\,m^{-2}\,h^{-1}$ for G1301-f, respectively. In Table 4 these values are listed as percentages of the uncorrected raw covariance.

The corrected fluxes were compared with methane flux calculated from TGA-100A data. This dataset should be almost free from density fluctuations and spectroscopic effects, since the closed-path analyzer was connected to a drier, while sampling line dampened temperature fluctuations. Therefore in theory with this kind of comparison it is possible to verify and assess the performance of WPL terms and spectroscopic corrections that were applied to RMT-200, G1301-f and Prototype-7700 data. Diurnal variation of TGA-100A methane flux is shown in Fig. 7 with diurnal variations of RMT-200, G1301-f and Prototype-7700 methane fluxes at different stages of post-processing. The diurnal variation of fully corrected flux agrees better with TGA-100A than the diurnal variation of not corrected flux. This is true for all three gas analysers, RMT-200, G1301-f and Prototype-7700. Therefore it can be said that both of the corrections are modifying

BGD
9, 17651–17706, 2012

the flux data into the right direction. For open-path Prototype-7700 WPL terms alone are not enough, due to the fact that diurnal variation of WPL-corrected Prototype-7700 flux differs quite a lot from the TGA-100A data at daytime. However, from Fig. 7 and Table 4 it is evident that the WPL terms are more significant for Prototype-7700 than the spectroscopic correction. After correcting the Prototype-7700 flux data with WPL terms high uptake of methane at daytime, i.e. flux directed downwards, is turned into weak emission which is more plausible at this site. Both corrections also increase the correlation between TGA-100A methane flux data and RMT-200, G1301-f and Prototype-7700 data. For RMT-200 methane flux data the correlation coefficient (r) with TGA-100A methane flux data is 0.75, 0.87 and 0.88 without WPL terms or spectroscopic correction, with WPL terms and with both corrections, respectively. For G1301-f methane flux data these correlation coefficients are 0.63, 0.89 and 0.89 and for Prototype-7700 they are −0.11, 0.10 and 0.22, respectively.

Negative value for the correction found for Prototype-7700 (Table 4) implies that the measured flux directed upwards is too large and it must be diminished. This kind of situations happens usually at night time when the water vapour flux is close to zero and temperature flux is directed downwards. If at the same time methane flux is directed upwards, as it is usually at this site, methane concentration and temperature fluctuations are negatively correlated with each other. Thus spectroscopic effects cause the fluctuations in methane concentration time series seem to be larger than they really are and measured methane flux is larger than the real flux. The opposite happens when the temperature flux is directed upwards: the fluctuation in methane concentration seem to be smaller than it really is and the methane flux is underestimated. This same reasoning applies also for water vapour flux induced apparent flux; however it is rarely, if ever, directed downwards. Thus spectroscopic correction caused by water vapour flux only increases the upwards directed methane flux, decreases downwards directed flux or has a negligible effect on the flux. Therefore spectroscopic correction for closed-path gas analyzers only increases the flux, if it is directed upwards, such as methane flux in this study. For open-path instruments the correction usually increases

BGD
9, 17651–17706, 2012

upwards directed daytime fluxes and decreases night time upwards directed fluxes (Fig. 7). However, this depends on the relative magnitude and direction of temperature and water vapour fluxes. These observations indicate that both WPL terms and spectroscopic correction are important, especially in the case of open-path gas analyzers.

3.5 Diurnal variation and methane flux magnitude

Mean diurnal variation of methane flux obtained from the four methane gas analyzers are shown in Fig. 8. Only data measured between 17 April and 17 May were used so that the figure can be compared with Table 5. The mean methane fluxes agree well at night. All the four measurement systems measuring methane flux show that the flux is on average between 0.3 and 0.4 $\mathrm{mg\,m^{-2}\,h^{-1}}$. While the measured methane fluxes agree at night, at daytime there is a bigger difference between them. Rinne et al. (2007) did not find any diurnal variation in methane flux at this measurement site. In our study none of the four gas analysers show a statistically significant diurnal pattern for the methane flux (Fig. 8), which is in line with Rinne et al. (2007). For Prototype-7700 it is difficult to assess the validity of methane flux diurnal variation due to high variation in the data.

By comparing the measured methane flux to the mean value of all the methane flux values, it is possible to assess the magnitude of the methane flux relative to each other. This kind of comparison can be seen in Tables 5 and 6. RMT-200 gives the highest methane fluxes between 17 April and 17 May (0.448 $\mathrm{mg\,m^{-2}\,h^{-1}}$), while Prototype-7700 gives the lowest (0.385 $\mathrm{mg\,m^{-2}\,h^{-1}}$).

3.6 Long-term performance

Figure 9 shows how well the methane flux estimates from the four methane gas analyzers agree with each other. Methane flux from G1301-f was selected as a reference for the three other gas analyzers because of two reasons: the random error was relatively small (Sect. 3.3) and the corrections to the flux measurements are small.

BGD
9, 17651–17706, 2012

RMT-200 and G1301-f methane fluxes agree well during low flux periods and high flux periods (Fig. 9). This can be seen from the fact that all the points are crowded in a narrow band near the 1 : 1 line and the scattering of the points is increased neither in the low flux nor in the high flux end of the figure. A linear regression was fitted to the measurements and the fit can be seen in the figure. Slope (0.997) and intercept (0.041) imply of good match between datasets. 95 % confidence intervals for the coefficient estimates are 0.996 and 0.999 for the slope and 0.036 and 0.045 for the intercept. The correlation coefficient between the datasets is high ($r = 0.999$) and the root mean square error is low (RMSE = 0.133). Functioning of the gas analysers RMT-200 and G1301-f are based on quite similar basic principle and this might explain the good correlation.

G1301-f does not agree as well with TGA-100A as it does with RMT-200 (Fig. 9). The slope of the fitted linear regression is 0.886 (95 % confidence intervals are 0.876 and 0.896) and it is clearly below the ideal slope of 1 : 1 line. The intercept is quite near zero with value of 0.005 (95 % confidence intervals are -0.027 and 0.036). However, most of the points follow the 1 : 1 line, but few outliers cause the fit to differ from the ideal 1 : 1 line. This can also be seen if the values of the residual are examined: they are mostly positive when the flux is large. If the fit describes the measurements well, the residual values should vary around zero, as in the case of RMT-200 and G1301-f methane fluxes. Thus, it can be argued that the TGA-100A and G1301-f methane flux datasets agree better than the slope of the fitted linear regression implies, at least when the flux is not exceedingly large. The correlation between the TGA-100A and G1301-f datasets ($r = 0.957$) is smaller than between RMT-200 and G1301-f methane fluxes and the root mean square error is higher (RMSE = 0.778). There was quite a lot of scattering in TGA-100A methane flux data and thus the points are not grouped as a narrow band around the fitted line and RMSE is rather high. The scattering in TGA-100A methane flux data is probably caused by high random error in the measurements (Sect. 3.3).

BGD
9, 17651–17706, 2012

Also the agreement between Prototype-7700 and G1301-f was assessed (Fig. 9), even though the amount of Prototype-7700 measurements is smaller than the amount of data received from the other gas analyzers. Prototype-7700 was operational only during period with relatively low methane flux, and thus the points in the scatter plot figure are near-zero. However, even though the points are located in a small range of methane flux values, it can be seen that they follow quite well the ideal 1 : 1 line. Fitted linear regression has slope and intercept of 1.054 (95 % confidence intervals are 0.976 and 1.133) and -0.107 (95 % confidence intervals are −0.184 and −0.031), respectively. The correlation coefficient between the Prototype-7700 and G1301-f methane flux datasets is 0.614 and root mean square error is 1.022. Low correlation and high RMSE are caused by scatter in the points when G1301-f measured quite low flux. Without these deviations from 1 : 1 line the correlation would be better. Scatter plots of methane flux data obtained only between 17 May and 17 April are shown on the right in Fig. 9.

Cumulative emission of methane during a part of the campaign (between 1 May and 25 October) was estimated from the data obtained from three closed-path gas analyzers, namely RMT-200, G1301-f and TGA-100A. They functioned with occasional breaks throughout the measurement campaign, while for Prototype-7700 the amount of received data was small, and cumulative flux data were not estimated. Cumulative emission was calculated from mean daily methane fluxes and the mean daily values were calculated from methane flux data which was flagged with quality flag 0. If less than one third of the measurements in a day fulfilled this criterion, mean daily methane flux was estimated using the dependence between methane flux and peat temperature (Eq. 16) and the same gap filling method was used for all the methane flux measurements. This kind of procedure lead 34, 68 and 103 out of 178 days to be gap filled for RMT-200, G1301-f and TGA-100A datasets, respectively. Cumulative methane emission estimated from RMT-200 data was based on measurements the most due to small amount of gap filled days, while TGA-100A had the most gap filled days. In fact, cumulative methane emission estimated from TGA-100A data is more based on gap filling

BGD
9, 17651–17706, 2012

than on real measurements, since the amount of gap filled days exceeds the amount of measured days and thus the value for methane balance estimated from TGA-100A data is a bit dubious.

The mean daily methane flux values show great similarity over the period and the gap filled values follow closely the measured values (upper part in Fig. 10). Only during the extremely high flux period around day of year 200 is not modelled well by the gap filling method. The three estimates for the cumulative emission shown in the lower part of Fig. 10 are almost the same and the amount of overall emitted methane over the period for RMT-200, G1301-f and TGA-100A data are 12.3 $g\,m^{-2}$, 12.0 $g\,m^{-2}$ and 11.8 $g\,m^{-2}$, respectively. Thus it can be said that the methane balance obtained from the three gas analyzers is the same even though the amount of gap filled days is not. Overall the daily methane emissions estimated from these three gas analyzers agree very well and the determination of methane balance does not depend on the selection of the gas analyzer.

4 Discussion and conclusions

Measurements obtained from methane gas analyzer intercomparison campaign held between 1 April and 26 October 2010 in Siikaneva fen were analyzed. Assessment of turbulent cospectra and power spectra revealed that white noise dominates a significant part of TGA-100A methane power spectra (Fig. 3), which is contrary to Billesbach et al. (1998), who show power spectra without any contamination of white noise. RMT-200 and G1301-f power spectra follows quite well the theoretical prediction (–2/3-slope) during high flux period (Fig. 3), while during low flux the spectra was greatly affected by white noise (not shown). Obtained RMT-200 power spectra at high flux period agrees with the spectra obtained for the same instrument by Tuzson et al. (2010) and Hendriks et al. (2008).

McDermitt et al. (2010) did not see white noise in their Prototype-7700 methane power spectra. Also Prototype-7700 power spectra in Detto et al. (2011) did not show

BGD
9, 17651–17706, 2012

significant contribution from white noise. The observed white noise might be caused by the fact that Prototype-7700 was operational only during a period with relatively low flux and thus the signal, meaning turbulence induced fluctuation in methane concentration, was not easily detectable. Possibly, during a high flux period the instrument could have performed better. Also high frequency signal attenuation (Fig. 6) was pronounced for Prototype-7700, while for the other three instruments the attenuation was more or less in the range that can be expected for closed-path gas analyzers. Again, McDermitt et al. (2010) disagrees with this study by showing production unit LI-7700 methane flux cospectra with smaller high frequency attenuation. Detto et al. (2011) show production unit LI-7700 methane cospectra which are attenuated a bit more than CO_2 and H_2O cospectra measured with LI-7500, and Dengel et al. (2011) show also a more attenuated methane cospectrum. High frequency variation in the signal should not be damped exceedingly when using open-path gas analyzers due to the fact that sampling tube is not needed. Therefore relatively long response time (0.16 s) obtained for Prototype-7700 is a bit surprising. The likely explanation for such high frequency attenuation is that Prototype-7700 was installed 0.45 m lower than sonic anemometer and intakes from other devices. Also there were wood log structure located 1–1.2 meters below the Prototype-7700 setup, but not below the three closed-path instruments and their anemometer. This likely caused the attenuated cospectra, longer response time, indicating that flux related to high frequency fluctuations was not fully measured, and without spectral corrections, the flux would have been underestimated. Possibly the size of the open measurement cell also contributed to the high frequency dampening of contribution from the smallest eddies. Overall, this is probably more related to the measurement setup than to the instrument performance.

When methane flux is small, approximately 0.3 $mg\,m^{-2}\,h^{-1}$ or smaller, TGA-100A and Prototype-7700 have difficulties in measuring the flux as precisely as higher fluxes, while precision of RMT-200 and G1301-f measurements were independent of the flux magnitude. In addition, RMT-200 and G1301-f methane fluxes had the smallest random errors, on average, and the distribution of absolute value of fractional flux error was

BGD
9, 17651–17706, 2012

narrow (Fig. 5). Interestingly the AFFE values are similar to values Finkelstein and Sims (2001) report for temperature flux measurements and for instance for CO_2-flux they report mean AFFE value of 0.25. Only TGA-100A methane flux had a similar mean AFFE value (Fig. 4). However this does not necessarily mean that the three other methane gas analyzers were more precise than the CO_2-analyser Finkelstein and Sims (2001) used. Sampling error depends on site characteristics and thus the values between these two studies are not entirely comparable. Detto et al. (2011) estimated instrumental noise in RMT-200 data to be larger than in Prototype-7700 data, while in this study Prototype-7700 had higher instrumental noise (Fig. 4). They estimated instrumental noise with the same method that was used in this study.

Open-path Prototype-7700 measurements were highly sensitive to water vapour and temperature contribution to WPL terms (Fig. 7 and Table 4) as expected for open-path design. Also Detto et al. (2011) reported that WPL terms had a major impact on the open-path measurements and they stress that this correction will eventually affect the precision of the flux estimates. In the middle of day, when water vapour and temperature fluxes were high, the WPL terms were of the same order of magnitude as the originally measured raw methane flux. Also spectroscopic correction had significant impact on Prototype-7700 methane fluxes; however the correction was smaller than density fluctuation induced errors, i.e. WPL terms. For closed-path RMT-200 and G1301-f, WPL terms and spectroscopic corrections were not as significant. For closed-path instruments, these two corrections are linearly dependent on water vapour flux. Therefore, even though the corrections were moderate for RMT-200 and G1301-f fluxes on average, they might have bigger effect on the measurements, when methane flux is low and water vapour flux is high. Spectral corrections had the biggest effect on RMT-200 methane fluxes, which was expected due to the fact that it had the longest response time. However, this is probably more related to the measurement setup than to the instrument performance.

Fully corrected fluxes from the four gas analyzers agree very well (Fig. 9), especially RMT-200 and G1301-f. Detto et al. (2011) showed rather good agreement between

BGD
9, 17651–17706, 2012

RMT-200 and Prototype-7700 fluxes which was also seen in this study (not shown). Also the long-term performance was assessed. Prototype-7700 was not in operation after 11 June 2010, and thus long-term performance of this instrument was not assessed. The daily methane fluxes calculated from the fully corrected flux values agree throughout the measurement period (Fig. 10) and the three estimates for methane balance are very similar. However, this can be at least partly caused by the fact that all the three methane flux time series were gap filled with the same method.

Overall, all the four gas analyzers performed quite well. The Prototype-7700 was in operation during 33 days in the beginning of the campaign, during the period with low CH_4 fluxes, and then was water damaged due to an unseal housing. The sealing was later redesigned for the production unit to resolve this issue. It had a larger AFFE value than the two other new instruments, RMT-200 and G1301-f (Fig. 4), which may be caused by the fact that the open measurement cell is sensitive to temperature and water vapour fluctuations which appear as high random error. Also, the WPL terms, spectroscopic and spectral corrections had a significant impact on the final flux, occasionally exceeding the raw covariance. However, these do not pose a problem for flux calculations if all the variables needed in the WPL terms and corrections are measured and applied. RMT-200 random errors were similar to G1301-f random errors. In addition RMT-200 was functioning quite stably throughout the measurement period, unlike G1301-f, which had a large gap in July–August. While the Prototype-7700 is lightweight and low-power instrument, making it a practical choice for measurement sites in remote locations, RMT-200 was the overall best performer in this intercomparison, making it a recommended choice for a new fast response methane gas analyzer in grid-powered sites.

Acknowledgements. We would like to thank LI-COR Biosciences for lending the early prototype of the LI-7700 instrument. For funding we thank Magnus Ehrnrooth foundation, the Academy of Finland Centre of Excellence program (project no 1118615), the Academy of Finland ICOS project (263149), Nordfrosk project DEFROST, EU projects ICOS and GHG-Europe.

BGD
9, 17651–17706, 2012

References

Aubinet, M., Grelle, A., Ibrom, A., Rannik, U., Moncrieff, J., Foken, T., Kowalski, A. S., Martin, P. H., Berbigier, P., Bernhofer, C., Clement, R., Elbers, J., Granier, A., Grunwald, T., Morgenstern, K., Pilegaard, K., Rebmann, C., Snijders, W., Valentini, R., and Vesala, T.: Estimates of the annual net carbon and water exchange of forests: the EUROFLUX methodology, Adv. Ecol. Res., 30, 113–175, 2000. 17657, 17658, 17659, 17674

Aurela, M., Riutta, T., Laurila, T., Tuovinen, J. P., Vesala, T., Tuittila, E. S., Rinne, J., Haapanala, S., and Laine, J.: CO_2 exchange of a sedge fen in Southern Finland – the impact of a drought period, Tellus B, 59, 826–837, 2007. 17654

Bär, D. S., Paul, J. B., Gupta, J. B., and O'Keefe, A.: Sensitive absorption measurements in the near-infrared region using off-axis integrated-cavity-output spectroscopy, Appl. Phys. B, 75, 261–265, 2002. 17654

Billesbach, D., Kim, J., Clement, R., Verma, S., and Ullman, F.: An intercomparison of two tunable diode laser spectrometers used for eddy correlation measurements of methane flux in a prairie wetland, J. Atmos. Ocean. Tech., 15, 197–206, 1998. 17653, 17682

Billesbach, D. P.: Estimating uncertainties in individual eddy covariance flux measurements: a comparison of methods and a proposed new method, Agr. Forest Meteorol., 151, 394–405, 2011. 17665, 17672, 17700

Burba, G., McDermitt, D., Komissarov, A., Anderson, T., Xu, L., and Riensche, B.: Method and apparatus for determining gas flux. US Patent 7953558: Filed 3 September 2009; Granted 31 May 2011. International Patent PCT/US2009/055936: Filed 3 September 2009; Granted 1 January 2010, 2009. 17661, 17662, 17663

Burch, D. E., Singleton, E. B., and Williams, D.: Absorption line broadening in the infrared, Appl. Optics, 1, 359–363, 1962. 17661

Businger, J. A.: Evaluation of the accuracy with which dry deposition can be measured with current micrometeorological techniques, J. Clim. Appl. Meteorol., 25, 1100–1124, 1986. 17664

Chen, H., Winderlich, J., Gerbig, C., Hoefer, A., Rella, C. W., Crosson, E. R., Van Pelt, A. D., Steinbach, J., Kolle, O., Beck, V., Daube B. C., Gottlieb, E. W., Chow V. Y., Santoni, G. W. and Wofsy, S. C.: High-accuracy continuous airborne measurements of greenhouse gases (CO_2 and CH_4) using the cavity ring-down spectroscopy (CRDS) technique, Atmos. Meas. Tech., 3, 375–386, 2010, http://www.atmos-meas-tech.net/3/375/2010/. 17663, 17676

BGD
9, 17651–17706, 2012

Conrad, R.: Control of Methane Production in Terrestrial Ecosystems, vol. 47, John Wiley & Sons Ltd, Chichester, 1989. 17666
Dengel, S., Levy, P. E., Grace, J., Jones, S. K., and Skiba, U. M.: Methane emissions from sheep pasture, measured with an open-path eddy covariance system, Global Change Biol., 17, 3524–3533, 2011. 17654, 17683
Detto, M., Verfaillie, J., Anderson, F., Xu, L., and Baldocchi, D.: Comparing laser-based open- and closed-path gas analyzers to measure methane fluxes using the eddy covariance method, Agr. Forest Meteorol., 151, 1312–1324, 2011. 17654, 17675, 17682, 17683, 17684
Drebs, A., Nordlund, A., Karlsson, P., Helminen, J., and Rissanen, P.: Climatological Statistics of Finland 1971–2000, Finnish Meteorological Institute, Helsinki, 2002. 17654, 17655
Eugster, W. and Pluess, P.: A fault-tolerant eddy covariance system for measuring CH_4 fluxes, Agr. Forest Meteorol., 150, 841–851, 2010. 17654
Finkelstein, P. and Sims, P.: Sampling error in eddy correlation flux measurements, J. Geophys. Res.-Atmos., 106, 3503–3509, 2001. 17664, 17665, 17684
Finnigan, J. J., Clement, R., Malhi, Y., Leuning, R., and Cleugh, H. A.: A re-evaluation of long-term flux measurement techniques – Part I: Averaging and coordinate rotation, Bound.-Lay. Meteorol., 107, 1–48, 2003. 17659
Foken, T. and Wichura, B.: Tools for quality assessment of surface-based flux measurements, Agr. Forest Meteorol., 78, 83–105, 1996. 17669, 17692
Goulden, M. L., Munger, J. W., Fan, S. M., Daube, B. C., and Wofsy, S. C.: Measurements of carbon sequestration by long-term eddy covariance: methods and a critical evaluation of accuracy, Global Change Biol., 2, 169–182, 1996. 17668
Hendriks, D. M. D., Dolman, A. J., van der Molen, M. K., and van Huissteden, J.: A compact and stable eddy covariance set-up for methane measurements using off-axis integrated cavity output spectroscopy, Atmos. Chem. Phys., 8, 431–443, doi:10.5194/acp-8-431-2008, 2008. 17654, 17682
Horst, T. W.: A simple formula for attenuation of eddy fluxes measured with first-order-response scalar sensors, Bound.-Lay. Meteorol., 82, 219–233, 1997. 17659
Ibrom, A., Dellwik, E., Flyvbjerg, H., Jensen, N. O., and Pilegaard, K.: Strong low-pass filtering effects on water vapour flux measurements with closed-path eddy correlation systems, Agr. Forest Meteorol., 147, 140–156, 2007. 17663
Kaimal, J. C. and Finnigan, J. J.: Atmospheric boundary layer flows: their structure and measurement, Oxford University Press, New York, 1994. 17658, 17699

BGD
9, 17651–17706, 2012

Kaimal, J. C., Wyngaard, J. C., Izumi, Y., and Cotè, O. R.: Spectral characteristics of surface-layer turbulence, Q. J. Roy. Meteor. Soc., 98, 563–589, 1972. 17699

Kroon, P. S., Schrier-Uijl, A. P., Hensen, A., Veenendaal, E. M., and Jonker, H. J. J.: Annual balances of CH_4 and N_2O from a managed fen meadow using eddy covariance flux measurements, Eur. J. Soil Sci., 61, 773–784, 2010. 17664, 17666

Leuning, R. and Moncrieff, J.: Eddy-covariance CO_2 flux measurements using open-path and closed-path CO_2 analyzers – corrections for analyzer water-vapor sensitivity and damping of fluctuations in air sampling tubes, Bound.-Lay. Meteorol., 53, 63–76, 1990. 17662

LI-COR Inc.: LI-7700 Open Path CH_4 Analyzer Instruction Manual, LI-COR Biosciences, Lincoln, USA, 2010.

Lübken, F. J., Eng, R., Karecki, D. R., Mackay, G. I., Nadler, S., and Schiff, H. I.: The effect of water-vapor broadening on methane eddy-correlation flux measurements, J. Atmos. Chem., 13, 97–108, 1991. 17661

Massman, W.: A simple method for estimating frequency response corrections for eddy covariance systems, Agr. Forest Meteorol., 104, 185–198, 2000. 17659

McDermitt, D., Burba, G., Xu, L., Anderson, T., Komissarov, A., Riensche, B., Schedlbauer, J., Starr, G., Zona, D., Oechel, W., Oberbauer, S., and Hastings, S.: A new low-power, open-path instrument for measuring methane flux by eddy covariance, Appl. Phys. B, 102, 391–405, 2010. 17654, 17656, 17661, 17662, 17663, 17675, 17676, 17682, 17683

Moncrieff, J. B., Massheder, J. M., deBruin, H., Elbers, J., Friborg, T., Heusinkveld, B., Kabat, P., Scott, S., Soegaard, H., and Verhoef, A.: A system to measure surface fluxes of momentum, sensible heat, water vapour and carbon dioxide, J. Hydrol., 189, 589–611, 1997. 17659

Moore, C. J.: Frequency-response corrections for eddy-correlation systems, Bound.-Lay. Meteorol., 37, 17–35, 1986. 17659

Neftel, A., Ammann, C., Fischer, C., Spirig, C., Conen, F., Emmenegger, L., Tuzson, B., and Wahlen, S.: N_2O exchange over managed grassland: application of a quantum cascade laser spectrometer for micrometeorological flux measurements, Agr. Forest Meteorol., 150, 775–785, 2010. 17661, 17662, 17663

O'Keefe, A. and Deacon, D. A. G.: Cavity ring-down optical spectrometer for absorption-measurements using pulsed laser sources, Rev. Sci. Instrum., 59, 2544–2551, 1988. 17656

Rannik, U. and Vesala, T.: Autoregressive filtering versus linear detrending in estimation of fluxes by the eddy covariance method, Bound.-Lay. Meteorol., 91, 259–280, 1999. 17659

BGD
9, 17651–17706, 2012

Rannik, U., Vesala, T., and Keskinen, R.: On the damping of temperature fluctuations in a circular tube relevant to the eddy covariance measurement technique, J. Geophys. Res.-Atmos., 102, 12789–12794, 1997. 17662

Rinne, J., Riutta, T., Pihlatie, M., Aurela, M., Haapanala, S., Tuovinen, J. P., Tuittila, E. S., and Vesala, T.: Annual cycle of methane emission from a boreal fen measured by the eddy covariance technique, Tellus B, 59, 449–457, 2007. 17653, 17657, 17666, 17667, 17679

Riutta, T., Laine, J., Aurela, M., Rinne, J., Vesala, T., Laurila, T., Haapanala, S., Pihlatie, M., and Tuittila, E. S.: Spatial variation in plant community functions regulates carbon gas dynamics in a boreal fen ecosystem, Tellus B, 59, 838–852, 2007. 17654

Rothman, L. S., Gordon, I. E., Barbe, A., Benner, D. C., Bernath, P. E., Birk, M., Boudon, V., Brown, L. R., Campargue, A., Champion, J. P., Chance, K., Coudert, L. H., Dana, V., Devi, V. M., Fally, S., Flaud, J. M., Gamache, R. R., Goldman, A., Jacquemart, D., Kleiner, I., Lacome, N., Lafferty, W. J., Mandin, J. Y., Massie, S. T., Mikhailenko, S. N., Miller, C. E., Moazzen-Ahmadi, N., Naumenko, O. V., Nikitin, A. V., Orphal, J., Perevalov, V. I., Perrin, A., Predoi-Cross, A., Rinsland, C. P., Rotger, M., Simeckova, M., Smith, M. A. H., Sung, K., Tashkun, S. A., Tennyson, J., Toth, R. A., Vandaele, A. C., and Auwera, J. V.: The HITRAN 2008 molecular spectroscopic database, J. Quant. Spectrosc. Ra., 110, 533–572, 2009. 17661

Schotanus, P., Nieuwstadt, F. T. M., and Debruin, H. A. R.: Temperature-measurement with a sonic anemometer and its application to heat and moisture fluxes, Bound.-Lay. Meteorol., 26, 81–93, 1983. 17658

Stull, R. B.: An Introduction to Boundary Layer Meteorology, 1 edn., Kluwer Academic Publishers, The Netherlands, 1988. 17664

Suyker, A., Verma, S., Clement, R., and Billesbach, D.: Methane flux in a boreal fen: season-long measurement by eddy correlation, J. Geophys. Res.-Atmos., 101, 28637–28647, 1996. 17653, 17666

Tuzson, B., Hiller, R. V., Zeyer, K., Eugster, W., Neftel, A., Ammann, C., and Emmenegger, L.: Field intercomparison of two optical analyzers for CH_4 eddy covariance flux measurements, Atmos. Meas. Tech., 3, 1519–1531, doi:10.5194/amt-3-1519-2010, 2010. 17653, 17654, 17661, 17662, 17663, 17676, 17682

Verma, S. B., Ullman, F. G., Billesbach, D. P., Clement, R. J., Kim, J., and Verry, E. S.: Eddy-correlation measurements of methane flux in a northern peatland ecosystem, Bound.-Lay. Meteorol., 58, 289–304, 1992. 17653

BGD
9, 17651–17706, 2012

Webb, E. K., Pearman, G. I., and Leuning, R.: Correction of flux measurements for density effects due to heat and water-vapor transfer, Q. J. Roy. Meteor. Soc., 106, 85–100, 1980. 17660, 17661, 17676

Wille, C., Kutzbach, L., Sachs, T., Wagner, D., and Pfeiffer, E. M.: Methane emission from Siberian arctic polygonal tundra: eddy covariance measurements and modeling, Global Change Biol., 14, 1395–1408, 2008. 17666

BGD

9, 17651–17706, 2012

Table 1. Characteristics of the four methane gas analyzers and their respective setups.

	Prototype-7700	G1301-f	TGA-100A	RMT-200
Analyser type	open-path analyser enhanced with WMS	WS-CRDS	TDLAS	off-axis ICOS
Open/closed path	open	closed	closed	closed
Measured species	CH_4	CH_4, H_2O	CH_4	CH_4
Sampling height above the soil	2.3 m	2.5 m	2.5 m	2.5 m
Sampling height above significant structures	1.1 m	2.5 m	2.5 m	2.5 m
Horizontal sensor separation	10 cm	5 cm	5 cm	5 cm
Vertical sensor separation	45 cm	25 cm	30 cm	25 cm
Leng sampling line	0 m	16.8 m	13 m	15 m
Flow rate	wind speed	10 LPM	14 LPM	12 LPM
Sample cell volume	open	33 cm^3	480 cm^3	408 cm^3
Sample cell pressure	ambient pressure	187 hPa	60 hPa	189 hPa
Connected to dryer	No	No	Yes	No
System power demand	low (solar- and wind-powered)	high (grid powered)	high (grid powered)	high (grid powered)
Need of maintenance	low	low	high	low

BGD
9, 17651–17706, 2012

Table 2. Amount of data obtained between 17 April and 17 May is given in the first two rows and in the three next rows the data is divided into bins according to data quality. Maximum number of data points during this period is 1440. Data with flag 0 include those periods when flux stationarity test Foken and Wichura (1996) was smaller than 0.3. Flag 1 corresponds to those periods when stationarity test was between 0.3 and 1 and flag 2 corresponds to stationarity test with value larger than 1.

	RMT-200	G1301-f	TGA-100A	Prototype-7700
Data (points)	1178	1173	1141	1045
Data (%)	82	81	79	73
Flag 0 (%)	77	77	61	56
Flag 1 (%)	4	3	13	12
Flag 2 (%)	1	1	5	5

BGD
9, 17651–17706, 2012

Table 3. Magnitude of spectral corrections given as percentages of raw uncorrected covariance. Positive and negative values mean that the correction increases upward and downward directed flux, respectively. Daytime was defined as periods when the sun's elevation angle was above 0° and night time was defined as periods when it was below −3°. Only data from a period when all the instruments were working (17 April–17 May) was used in calculating the values in the table.

	RMT-200	G1301-f	TGA-100A	Prototype-7700
All data (%)	11.1	6.6	5.4	3.5
Daytime (%)	12.1	7.4	6.2	−3.6
Night time (%)	9.1	5.3	4.1	7.3

BGD
9, 17651–17706, 2012

Table 4. WPL terms and spectroscopic correction given as percentages of the uncorrected raw covariance. Positive and negative values mean that the correction increases the upward and downward directed flux, respectively. Daytime was defined as those periods when sun's elevation angle was above 0° and night time as those periods when it was below −3°. Only data from a period when all the instruments were working (17 April–17 May) was used in calculating the values in the table.

		RMT-200	G1301-f	Prototype-7700
All data	WPL terms (%)	15.3	21.4	80.1
	Spectroscopic correction (%)	3.2	0.9	23.6
Daytime	WPL terms (%)	23.9	39.2	105.1
	Spectroscopic correction (%)	5.0	1.2	31.8
Night time	WPL terms (%)	4.5	7.0	−27.9
	Spectroscopic correction (%)	0.9	0.6	−8.5

BGD
9, 17651–17706, 2012

Table 5. Average difference between methane flux obtained from one instrument and mean flux obtained from the four instruments between 17 April and 17 May. All the four methane gas analyzers were working during this period. If difference and relative difference are negative, the flux obtained from that certain instrument is smaller than the mean flux obtained from all of the instruments. Only data flagged with quality flag 0 was used.

	RMT-200	G1301-f	TGA-100A	Prototype-7700
Flux ($mg\,m^{-2}\,h^{-1}$)	0.448	0.430	0.395	0.385
Difference ($mg\,m^{-2}\,h^{-1}$)	0.034	0.015	−0.020	−0.030
Relative difference (%)	7.6	3.6	−5.0	−7.7

BGD
9, 17651–17706, 2012

Table 6. Same as Table 5, but data was selected from between 9 June and 29 June. Prototype-7700 was out of operation during this period.

	RMT-200	G1301-f	TGA-100A
Flux ($mg\,m^{-2}\,h^{-1}$)	3.164	3.147	2.763
Difference ($mg\,m^{-2}\,h^{-1}$)	0.139	0.122	−0.261
Relative difference (%)	4.4	3.9	−9.4

BGD
9, 17651–17706, 2012

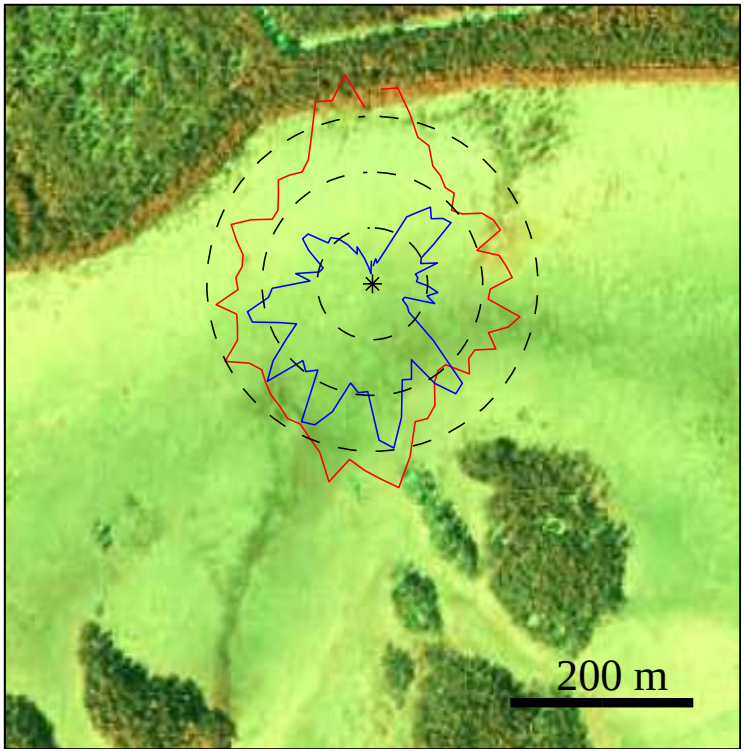

Fig. 1. Aerial photograph of the measurement site. Light green area shows area governed by the fen and the darker green area represents the surrounding forest. Star marks location of the measurement tower, red and blue lines show average methane flux and amount of obtained methane flux data as a function of wind direction, respectively. Methane flux is in units $mg\,m^{-2}\,h^{-1}$ and dashed lines show where methane flux equals 1, 2 and $3\,mg\,m^{-2}\,h^{-1}$ and amount of data equals 60, 120 and 180 points. Data obtained from RMT-200 was used in this plot.

BGD
9, 17651–17706, 2012

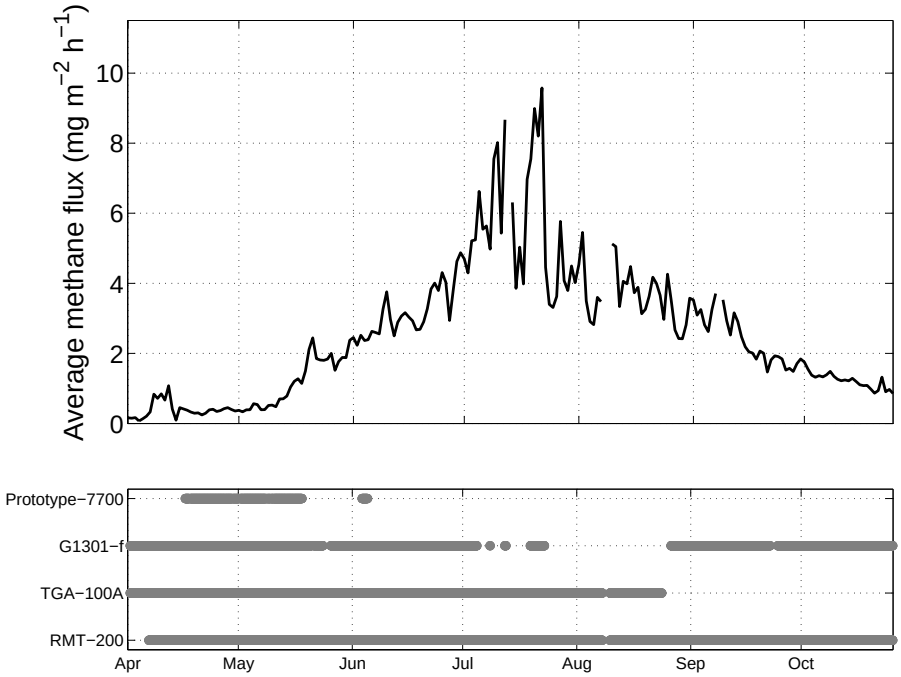

Fig. 2. Variation of methane flux obtained from the four instruments on average is shown in the upper figure and the periods when the methane gas analyzers were working are shown in the lower figure.

BGD
9, 17651–17706, 2012

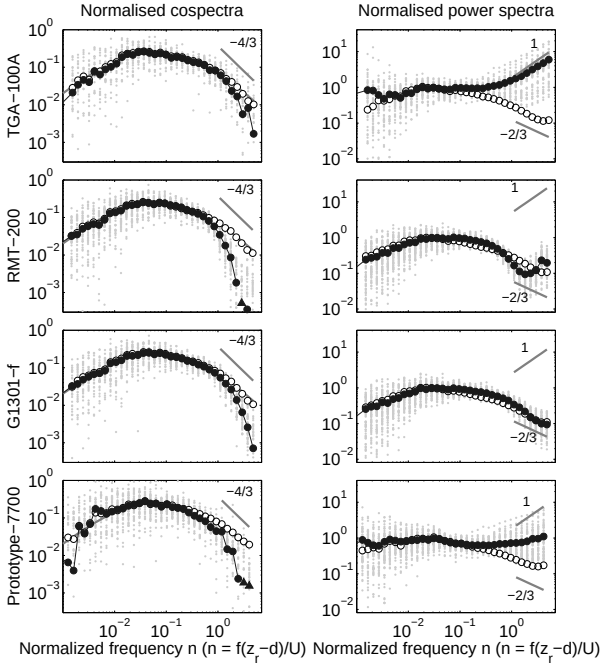

Fig. 3. Frequency weighted, normalized cospectra and power spectra plotted against normalized frequency *n*. The ensemble averaged methane and temperature cospectra and power spectra are shown with black and white dots, respectively. Black triangles represent negative points of the ensemble averaged methane cospectrum. Small grey dots represent individual methane data from which the mean cospectra and power spectra are calculated from. Straight line in the figures on the left indicates a slope of −4/3 (Kaimal et al., 1972). Lower and upper straight lines in the figures on the right correspond to ideal slope of −2/3 and 1, respectively. Slope of 1 is a sign of white noise (Kaimal and Finnigan, 1994). Cospectra were normalized with corresponding covariance and power spectra were normalized with variance values calculated between frequencies 0.005 Hz and 0.1 Hz. Spectral data was binned into 35 logarithmically evenly spaced bins before plotting. For Prototype-7700 data was selected from period 17 April–17 May, when methane flux was on average 0.5 $mg\,m^{-2}\,h^{-1}$, while for other gas analyzers the data was selected from period 9–29 June, when methane flux was on average 3.4 $mg\,m^{-2}\,h^{-1}$.

BGD
9, 17651–17706, 2012

Intercomparison of four EC methane gas analysers

O. Peltola et al.

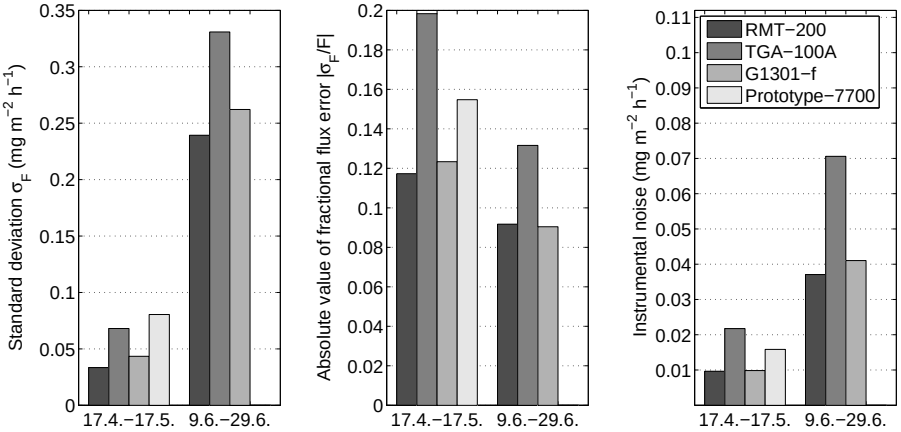

Fig. 4. From left to right: standard deviation of the covariances, absolute value of fractional flux error ($|\sigma_F/F|$) and instrumental noise. Median values for these three statistical parameters were calculated during two separate periods. Fractional flux error is calculated as a ratio between the standard deviations and the flux values. Instrumental noise was estimated using method proposed by Billesbach (2011).

BGD
9, 17651–17706, 2012

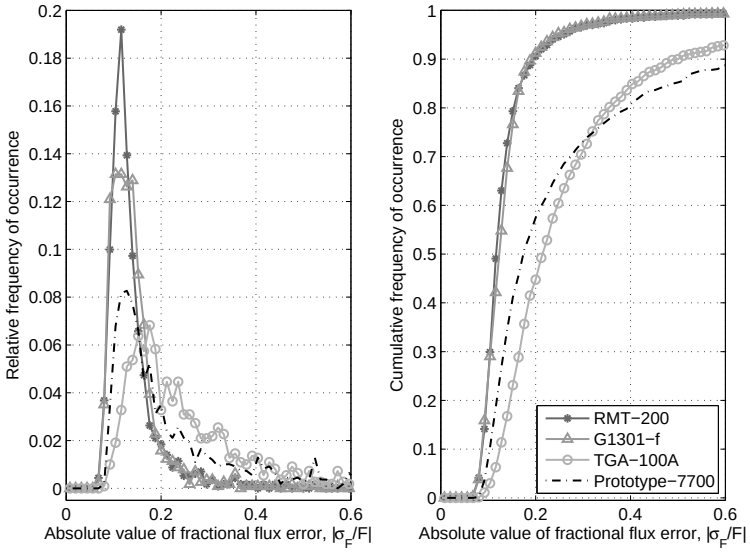

Fig. 5. Distribution curves of absolute value of fractional flux error ($|\sigma_F/F|$) are shown on the left and cumulative sums of relative frequency of occurrence are shown on the right. Frequency of occurrence is normalized with the amount of measurements and thus the curves on the left give relative amount of data in each AFFE bin. Only periods when all the methane gas analyzers were working were used.

BGD
9, 17651–17706, 2012

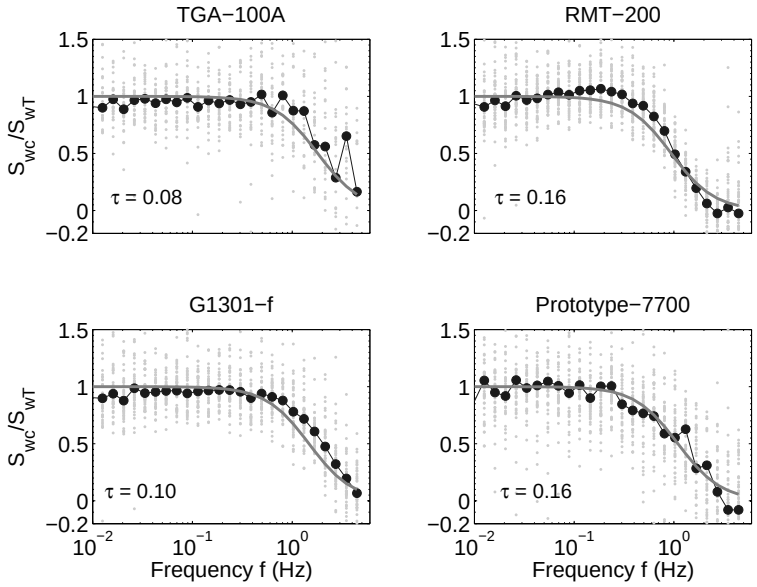

Fig. 6. Transfer function determined from measured cospectra. Grey line is transfer function (Eq. 4), black dots connected with a line represents mean methane cospectrum (S_{wc}) divided with mean temperature cospectrum (S_{wT}), grey dots show individual methane cospectra divided with corresponding temperature cospectra. Response times related to each gas analyzer are shown in the figure. Cospectral data was binned into 35 logarithmically evenly spaced bins before plotting. For Prototype-7700 data were selected from a period 17 May–17 April using the same selection criteria as in Sect. 3.2, while for the other gas analyzers data were selected from a period 9–29 June.

BGD
9, 17651–17706, 2012

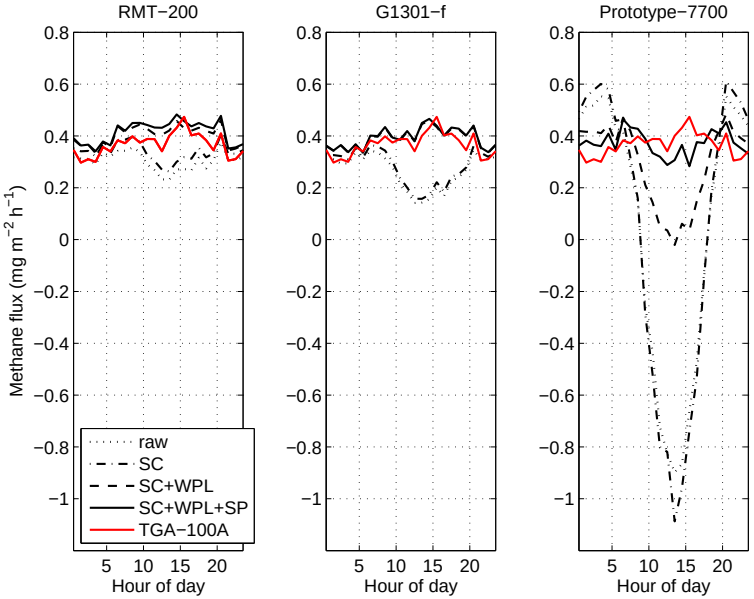

Fig. 7. Diurnal variations of RMT-200, G1301-f and Prototype-7700 methane fluxes at different stages of post-processing. Dotted line represents diurnal variation of raw, uncorrected data. SC, WPL and SP correspond to spectral corrections, WPL terms and spectroscopic correction, respectively. Therefore black line shows the diurnal variation of fully corrected, final flux. Diurnal variation of TGA-100A methane flux is shown for comparison with red line. Only data between 17 April and 17 May were used. Flux data flagged with quality flag 0 was selected for both plots individually and thus the red lines are not exactly the same in these two figures.

BGD
9, 17651–17706, 2012

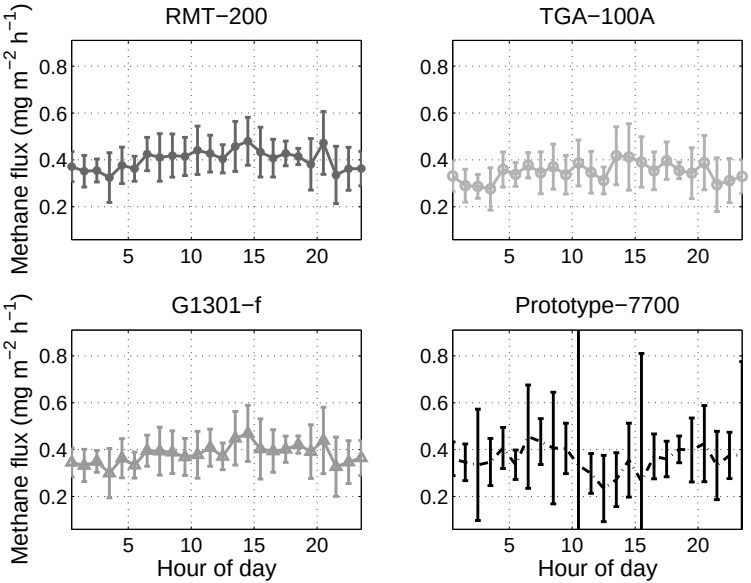

Fig. 8. Median diurnal variation of final fully corrected methane flux obtained from the four methane gas analyzers. Only data from a period when all the instruments were working (17 April–17 May) were used. Data from this period was selected so that the methane fluxes were given quality flag 0. Errorbars denote one standard deviation around the mean values.

BGD
9, 17651–17706, 2012

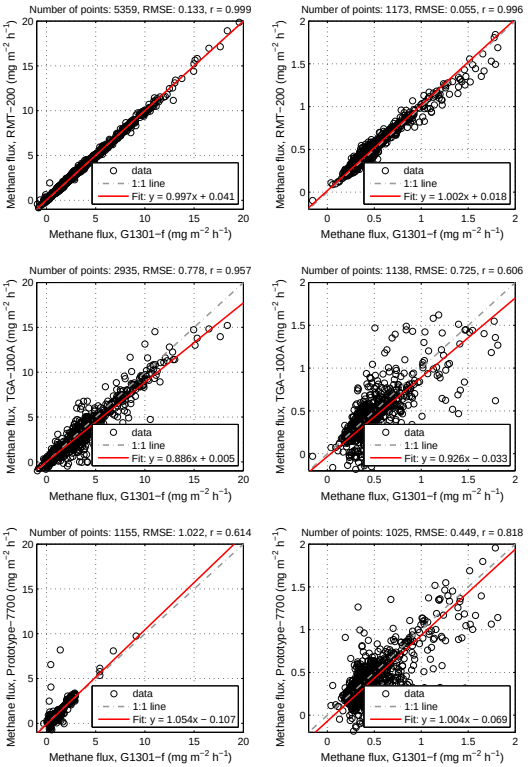

Fig. 9. Scatter plots of methane flux measured with different gas analyzers. Only periods when amount of spikes in a half an hour exceeded 100 were discarded. Number of points in the figure, root mean square error and correlation coefficient are given above each figure, respectively. Figures on the left show all the available data and figures on the right are otherwise similar, except data was selected only from period 17 May–17 April. During this period all the instruments were working simultaneously and methane flux was on average 0.5 $\mathrm{mg\,m^{-2}\,h^{-1}}$.

BGD
9, 17651–17706, 2012

Intercomparison of four EC methane gas analysers

O. Peltola et al.

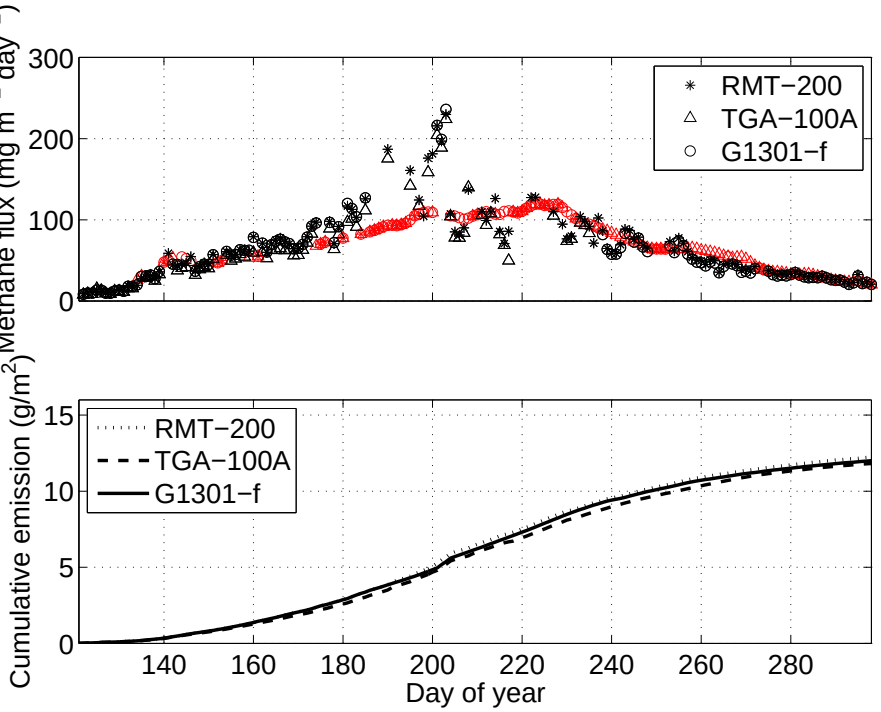

Fig. 10. Gap filled daily averaged methane flux is shown in the upper part and cumulative methane emission estimated from three gas analyzers is shown in the lower part. Black and red markers in the upper part represent measured and gap filled values, respectively.

BGD
9, 17651–17706, 2012